Geostationary satellite retrievals of aerosol optical thickness during ACE-Asia

Jun Wang,[1] Sundar A. Christopher,[1] Fred Brechtel,[2] Jiyoung Kim,[3] Beat Schmid,[4] Jens Redemann,[4] Philip B. Russell,[5] Patricia Quinn,[6] and Brent N. Holben[7]

Received 27 February 2003; revised 23 April 2003; accepted 13 May 2003; published 30 August 2003.

[1] Using 30 days of hourly geostationary satellite (GMS5 imager) data and discrete ordinate radiative transfer (DISORT) calculations, aerosol optical thickness (AOT) at 0.67 μm was retrieved over the west Pacific Ocean (20°N–45°N, 110°E–150°E) during the Aerosol Characterization Experiment (ACE-Asia) intensive observation period in April 2001. Different from previous one-channel retrieval algorithms, we have developed a strategy that utilizes in situ and ground measurements to characterize aerosol properties that vary both in space and time. Using Mie calculations and bilognormal size distribution parameters inferred from measurements, the relationship between Ångström exponent (α) and the ratio of two volume lognormal modes (γ) was obtained. On the basis of spectral AOT values inferred from the Aerosol Robotic Network (AERONET) sites, NASA Ames Airborne Sun photometers (AATS6 and AATS14) and a Sun photometer on board a ship, a successive correction method (SCM) was used to infer the spatial distribution of α in the study area. Comparisons between the satellite-retrieved AOT and AERONET values over four sites show good agreement with linear coefficients (R) of 0.86, 0.85, 0.86, and 0.87. The satellite-derived AOTs are also in good agreement with aircraft (R = 0.87) and ship measurements (R = 0.98). The average uncertainty in our AOT retrievals is about 0.08 with a maximum value of 0.15 mainly due to the assumptions in calibration (±0.05), surface reflectance (±0.01–±0.03), imaginary part of refractive index (±0.05), and SCM-derived α values (±0.02). The monthly mean AOT spatial distribution from GMS5 retrievals in April 2001 clearly shows the transport pattern of aerosols with high AOT near the coast of east Asia and low AOT over the open ocean. Using high temporal resolution satellite data, this paper demonstrates that the diurnal variation in AOT can be retrieved by current generations of geostationary satellites. The next generation of geostationary satellites with better spectral, spatial and radiometric resolution will significantly improve our ability to monitor aerosols and quantify their effects on regional climate. *INDEX TERMS:* 0305 Atmospheric Composition and Structure: Aerosols and particles (0345, 4801); 3360 Meteorology and Atmospheric Dynamics: Remote sensing; 4801 Oceanography: Biological and Chemical: Aerosols (0305); *KEYWORDS:* ACE-Asia, GMS, geostationary satellites, aerosol retrieval, aerosol optical thickness, dynamic aerosol model

Citation: Wang, J., S. A. Christopher, F. Brechtel, J. Kim, B. Schmid, J. Redemann, P. B. Russell, P. Quinn, and B. N. Holben, Geostationary satellite retrievals of aerosol optical thickness during ACE-Asia, *J. Geophys. Res.*, *108*(D23), 8657, doi:10.1029/2003JD003580, 2003.

1. Introduction

[2] The significance of aerosols in the climate system has been emphasized in many studies [*Charlson et al.*, 1992; *Kiehl and Briegleb*, 1993; *Boucher and Anderson*, 1995; *Schwartz*, 1996; *Hansen et al.*, 1997; *Ramanathan et al.*, 2001; *Kaufman et al.*, 2002]. The aerosol radiative forcing at the top of atmosphere (TOA) is comparable in magnitude to current anthropogenic greenhouse gas forcing (2.5 ± 0.5 Wm^{-2}) but opposite in sign [*Houghton et al.*, 1990]. Current estimates of aerosol forcing range from 0.5 to -4 Wm^{-2}, with uncertainties of at least ±100%, mainly due to lack of adequate information on the diurnal and spatial distribution of aerosols and their associated proper-

[1]Department of Atmospheric Sciences, University of Alabama, Huntsville, Alabama, USA.
[2]Brechtel Manufacturing Inc., Hayward, California, USA.
[3]Meteorological Research Institute, Seoul, South Korea.
[4]Bay Area Environmental Research Institute, Sonoma, California, USA.
[5]NASA Ames Research Center, Moffett Field, California, USA.
[6]Pacific Marine Environmental Laboratory, NOAA, Seattle, Washington, USA.
[7]Biospheric Sciences Branch, NASA Goddard Space Flight Center, Greenbelt, Maryland, USA.

0148-0227/03/2003JD003580$09.00

ties [*Intergovernmental Panel on Climate Change* (*IPCC*), 2001].

[3] To reduce uncertainties in the estimation of aerosol radiative forcing, one of the key parameters that must be accurately quantified is aerosol optical thickness (AOT) which is a measure of the aerosol extinction on radiative transfer [*Charlson et al.*, 1992; *Chylek and Wong*, 1995; *Russell et al.*, 1997]. Various methods have been used to infer the distribution and magnitude of AOT including ground-based Sun photometers (SP) [*Holben et al.*, 1998], lidar [*Welton et al.*, 2002] and aircraft [*Russell et al.*, 1999] measurements. Satellite measurements and retrievals from the AVHRR [e.g., *Rao et al.*, 1989; *Mishchenko et al.*, 1999; *Husar et al.*, 1997; *Higurashi and Nakajima*, 1999], TOMS [*Torres et al.*, 2002], SeaWiFS [*Higurashi and Nakajima*, 2002], POLDER [*Deuze et al.*, 1999], MODIS [*Kaufman et al.*, 1997; *Tanré et al.*, 1997] and MISR [*Kahn et al.*, 1997] are critical for studying the global aerosol effects on climate. Although the AOT inferred from point measurements and aircraft measurements are accurate, these observations are limited in space and time. Satellite measurements, due to their large spatial coverage (e.g, polar orbit satellite) and high temporal resolution (e.g., geostationary satellite), provide a unique tool for quantifying aerosol properties and spatial distributions. However, to reliably retrieve aerosol properties from satellite measurements, ground and aircraft measurements are needed to constrain the satellite retrieval processes and validate the satellite results. This study demonstrates such a strategy, with emphasis on estimating the day-time diurnal change of aerosol radiative forcing, by using geostationary satellite data and other measurements during the ACE-Asia Intensive Observation Period (IOP), 1–30 April 2001 [*Huebert et al.*, 2003].

[4] ACE-Asia was conducted off the coast of east China, Korea, and Japan from late March to early May 2001. A detailed description of this campaign is given by *Huebert et al.* [2003]. Observations show that dust aerosols from the Takla Makan and Gobi deserts in northwest China can be transported to Korea [*Chun et al.*, 2001a, 2001b], Japan [*Murayama et al.*, 2001], and even across the Pacific Ocean to the United States [*Husar et al.*, 2001; *Herman et al.*, 1997] and Canada [*McKendry et al.*, 2001]. Owing to rapid economic growth, the emission of industrial pollutants has increased in the east Asian regions [*Bergin et al.*, 2001]. The aerosols in this region include sulfate, dust, soot and sea salt, in a highly mixed condition, producing a complex aerosol loading in the troposphere [*Chun et al.*, 2001a; *Bergin et al.*, 2001; *Higurashi and Nakajima*, 2002]. Some studies have shown that aerosols might be an important factor for the regional cooling in the Sichuan basin in southern China [*Luo et al.*, 2001; *Li et al.*, 1995] and drought in northern China [*Menon et al.*, 2002].

[5] The focus of this study is to retrieve the diurnal change of AOT with special emphasis on characterizing the aerosol optical properties (i.e., a combination of both the chemical (composition and refractive index) and microphysical (size distribution) properties) by combining ground, ship and aircraft measurements. In contrast with the time-invariant aerosol models used in previous satellite retrieval studies [e.g., *Wang et al.*, 2003; *Zhang et al.*, 2001; *Rao et al.*, 1989], aerosol properties are calculated as a function of space and time (called the dynamic aerosol model) by incorporating an aerosol climatology for East Asia as well as observed aerosol properties from ground and in situ measurements during ACE-Asia.

2. Data and the Area of Study

[6] This study utilizes the AOT inferred from different platforms in the same study region including 12 ground-based Sun photometers (SP) at different AERONET sites; 6-channel Ames Airborne Tracking Sun photometer (AATS6) on board the C130 aircraft [*Redemann et al.*, 2003]; 14-channel AATS (AATS14) on board the CIRPAS Twin Otter aircraft [*Schmid et al.*, 2003]; and a Sun photometer on board the NOAA R/V *Ron Brown* (P. K. Quinn et al., Aerosol optical properties measured on board the *Ronald H. Brown* during ACE-Asia as a function of aerosol chemical composition and source region, submitted to *Journal of Geophysical Research*, 2003, hereinafter referred to as Quinn et al., submitted manuscript, 2003). The aerosol size distribution measured at the surface at the Gosan supersite, Cheju Island, Korea is also used. The hourly GMS5 Visible and Infra-Red Spin Scan Radiometer (VISSR) data are used to detect aerosols and retrieve AOTs.

[7] Figure 1 shows the area of study and the location of the AERONET sites. Twelve Sun photometers (SP) were used to build the monthly mean aerosol properties in April. Nine of these sites were operational during the ACE-Asia IOP 2001 (see Table 1), while the other three were operational in April of other years. At each site, the SP measured direct solar irradiance at 340 nm, 380 nm, 440 nm, 500 nm, 670 nm, 870 nm, and 1020 nm [*Holben et al.*, 1998]. Using a cloud screening process and an algorithm based on the Beer-Lambert-Bouguer law, the measured solar radiance is used to infer the column AOT [*Smirnov et al.*, 2000; *Holben et al.*, 1998]. The attenuation due to Rayleigh scattering and the absorption of ozone are estimated and removed. The uncertainty in the retrieved AOT is on the order of 0.01 [*Smirnov et al.*, 2000]. This study also uses the AOT inferred from a 5-channel (380, 440, 500, 675, and 870 nm) hand held Microtops Sun photometer on the R/V *Ron Brown* ship (Quinn et al., submitted manuscript, 2003). The main cruise route of the ship is shown as a dotted line in Figure 1. A Matlab routine used by the NASA SIMBIOS program and Brookhaven National Laboratory was used to convert the Sun photometer raw signal voltages to AOT. Included in the conversion is a correction for Rayleigh scattering, ozone optical depth, and an air mass that accounts for Earth's curvature (Quinn et al., submitted manuscript, 2003). The uncertainty in the Microtops Sun photometer AOT is less than 0.01 (Quinn et al., submitted manuscript, 2003). The AATS14 deployed on the Twin Otter and the AATS6 on the C-130 continuously measured the column optical depth between the aircraft and the top of the atmosphere (TOA) during research flights. By subtracting the AOT due to Rayleigh scattering of gas molecules and absorption by O_3, NO_2, H_2O, and O_2-O_2 [*Redemann et al.*, 2003; *Schmid et al.*, 2003; *Livingston et al.*, 2003], the AOT throughout the column of air between the altitude of the aircraft and the TOA is calculated. In this study, to compare with satellite column retrievals, only the AOT values that were measured near the surface were used (i.e., altitude below 100 m). Dry

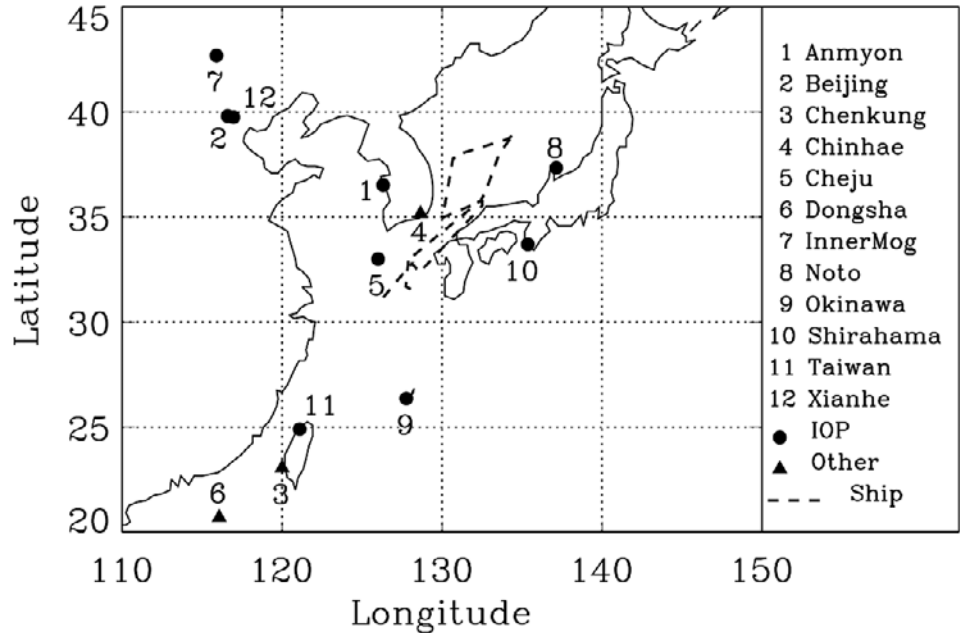

Figure 1. Study area and 12 Sun photometer (SP) sites used in this study. Also shown is the ship route during 3–16 April 2001. The filled circles are the sites where SP was operational during ACE-Asia. The filled triangles are the sites where SP were operational during the period other than IOP and were used to infer the aerosol climatology in this region.

aerosol size distributions at Gosan, Korea, measured with a ground-based twin-scanning electrical mobility sizing (TSEMS, 0.005–0.6 μm) system [*Brechtel and Buzorius*, 2001] and optical particle counters (OPC, 0.1–20 μm) [*Chun et al.*, 2001b] were used to constrain the input particle distribution used by the retrieval algorithm.

[8] Hourly GMS5 VISSR data are used in this study. Table 2 lists the GMS5 daytime observation periods and the number of GMS5 images in each corresponding time period. The VISSR has four channels; channel 1 (ch1) with a spectral range between 0.45 and 1.1 μm, ch2 between 10.1 and 11.5 μm, ch3 between 10.5 and 12.6 μm, and ch4 between 6.5 and 7.3 μm [*MSC*, 1997]. Although the visible channel (ch1) covers a large wavelength range from 0.45 to 1.1 μm, its major spectral response (>85%) is centered at 0.75 μm with bandwidth from 0.6 to 0.9 μm [*Meteorological Satellite Center* (*MSC*), 1997]. The VISSR has a spatial resolution (at nadir) of 1.25 × 1.25 km^2 in ch1, and 5 × 5 km^2 in other channels [*MSC*, 1997]. In our data archive, ch1 data was resampled to 5 km to match the spatial resolution of other channels. Although the original GMS5 VISSR data has a radiometric resolution of 6 bits, it is usually stretched to 8 bits (S-VISSR) and made available to the user community [*Marshall et al.*, 1999; *MSC*, 1997]. In this study, imager data from ch1, ch2 and ch3 with radiometric resolution of 8 bits and with a spatial resolution of 5 km (i.e., S-VISSR data) are used. The digitized data are converted into albedo and brightness temperature using the International Satellite Cloud Climatology Project (ISCCP) calibration coefficients [*Brest et al.*, 1997; *Desormeaux et al.*, 1993]. The retrieval errors in AOT due to calibration uncertainties are discussed in section 5.

3. Methodology

[9] Our retrieval method is based on a lookup table (LUT) approach [*Christopher and Zhang*, 2002; *Wang et al.*, 2003]. In noncloudy conditions, the reflectance at the top of atmosphere (TOA) in the visible spectrum mainly is a function of Sun-satellite geometries (i.e., solar zenith angle θ_0, viewing zenith angle θ, and relative azimuth angle ϕ), surface reflectance ρ_0, AOT, and aerosol optical properties (AOP). Since the Sun-satellite geometry is known for each satellite pixel, and the reflectance of the ocean surface can be obtained through analysis of satellite data [*Wang et al.*, 2003], the key aspect in satellite retrievals is to accurately model the aerosol optical properties that are primarily determined by the particle refractive index, size distribution and shape. There are at least 3 major unknowns in the retrieval algorithms, including the complex indices of refraction, size distribution and AOT. Traditional one-channel retrieval algorithms can only retrieve one parameter (e.g., AOT), whereas all the other parameters must be known priori [*Mishchenko et al.*, 1999]. Multiple channels however

Table 1. Location of Nine AERONET Sites During ACE-Asia IOP[a]

Name	Anmyon	Beijing	Cheju	InnterMog	Noto	Okinawa	Shirahama	Taiwan	Xianhe
Latitude, N	36.52	39.8	33	42.68	137.14	127.77	33.69	24.9	39.75
Longitude, E	126.32	116.6	126	115.95	37.33	26.36	135.36	121.1	116.96
Total points	633	410	499	200	358	23	289	46	399

[a]Also listed are the data points of each site during the GMS observation time period (see Table 2).

Table 2. Summary of GMS-5 Data Used in This Study

Number of Images	Observation Time, UTC
22	0132
24	0232
22	0332
19	0425
23	0732
23	2225
20	2302

can provide more information on aerosol spectral characteristics, and therefore can retrieve more aerosol parameters and improve the retrieval accuracy [*Tanré et al.*, 1997; *Higurashi and Nakajima*, 2002, 1999; *Mishchenko et al.*, 1999; *Kaufman et al.*, 1997]. For example, in glint-free ocean scenes, the MODIS with its multi spectral capabilities simultaneously retrieves spectral AOT, effective radii and the ratio between different size modes (e.g., fine versus coarse) [*Remer et al.*, 2002].

[10] The GMS5 has one visible channel and to retrieve AOT, aerosol optical properties must be properly characterized. Several studies have used a fixed (i.e., spatial-temporal independent) aerosol model [*Wang et al.*, 2003; *Zhang et al.*, 2001; *Christopher and Zhang*, 2002; *Moulin et al.*, 1997; *Ignatov et al.*, 1995] to infer the AOT information in an environment dominated by one aerosol type. However, due to the complexity of the aerosol in the east Asian region, it is neither sufficient nor reasonable to use a fixed aerosol model to calculate the aerosol optical properties. Therefore we have developed a dynamical aerosol model that can calculate the aerosol optical properties as a function of space and time. This model is implemented into the satellite retrieval algorithms to infer the AOT.

3.1. Dynamical Aerosol Model

[11] *Remer and Kaufman* [1998] built a dynamic model for smoke aerosols in which aerosol properties (such as size distribution and phase function) varied as a function of aerosol optical thickness. However, this approach is not suitable for this study, since our goal is to retrieve the AOT from satellite observations. Therefore needed parameters from measurements other than GMS-5 must be determined and used to characterize the aerosol optical properties dynamically. *Reid et al.* [1999] showed that the Ångström exponent α was well correlated with the aerosol size distributions, aerosol single scattering albedo and backscattering ratio, and proposed using α to estimate the variability in aerosol properties ($\alpha = -\ln(\tau_1/\tau_2)/\ln(\lambda_1/\lambda_2)$, where τ_1 and τ_2 are AOT at wavelength λ_1 and λ_2). The Ångström exponent α is also an important parameter in the two channel AHVRR retrieval algorithms [*Mishchenko et al.*, 1999; *Higurashi and Nakajima*, 1999] and is closely related to relative importance of fine versus coarse aerosols in the aerosol size distributions [*Tomasi et al.*, 1983]. Therefore

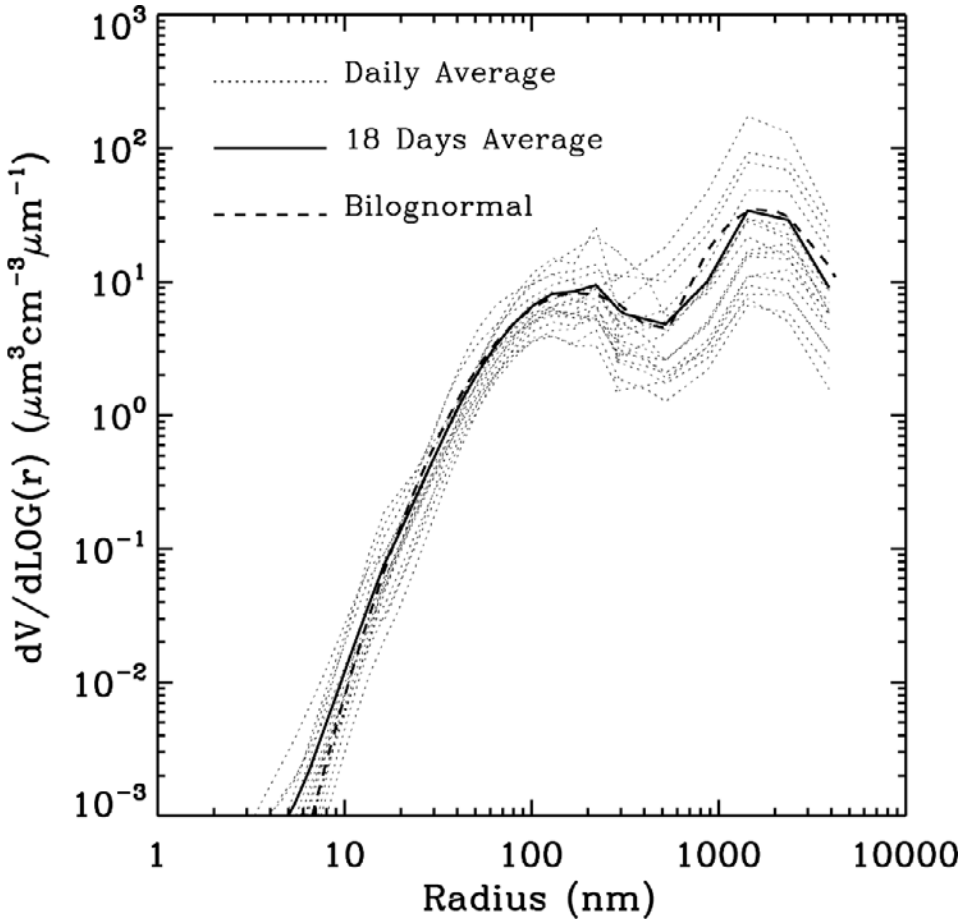

Figure 2. Volume size distribution measured in Gosan, Korea, from 10 to 27 April 2001. Also shown is the simulated bilognormal size distribution.

this study employs Ångström exponent as an index to model the variability of aerosol optical properties.

[12] The aerosol size distribution used in this study is inferred from ground-based twin-scanning electrical mobility sizing (TSEMS) and optical particle counter (OPC) measurements at Gosan, Korea [*Chun et al.*, 2001b; *Brechtel and Buzorius*, 2001]. Previous studies have demonstrated that the aerosol size distribution can be simulated by combining several lognormal size distributions [*d'Almeida et al.*, 1991]. Figure 2 shows the measured daily mean as well as the 18-day mean volume size distribution at Gosan. Figure 2 also shows a bilognormal pattern in the measured size distribution. For a given day, particle volume distribution can be computed as:

$$\frac{dV}{d\log_{10} r} = \sum_{n=1}^{2} C_n \exp\left[-\frac{1}{2}\left(\frac{\log_{10} r - \log_{10} r_{vn}}{\log_{10} \sigma_n}\right)^2\right], \quad (1)$$

where subscript n indicates the mode number; and r_{vn}, σ_n and C_n are the volume median radius, standard deviation and the peak of nth mode, respectively. In this study, r_{vn} value of 0.18 μm and 1.74 μm, σ_n of 2.16 and 1.78 were derived by fitting equation (1) to the 18-days mean size distribution (Figure 2) to represent the first and second mode, respectively.

[13] To use α as an index to model the variation of aerosol size distributions, a relationship between α and the size distribution must be established. Several studies have shown that α is closely related to the aerosol size distributions [e.g., *Tomasi et al.*, 1983; *Reid et al.*, 1999]. By assuming that aerosols have a Junge distribution $d\mathrm{N}/d\ln(\mathrm{r}) = \mathrm{r}^{-\nu}$ [*Junge*, 1955], we can show that $\alpha = \nu - 2$ [*Liou*, 2002]. However, the relationship between α and the size distribution may vary if aerosol size distribution does not follow a Junge size distribution [*Tomasi et al.*, 1983]. Figure 2 shows that the measured aerosol size distribution has a distinct bilognormal pattern where the mode parameters (i.e., r_{vn}, σ_n) have little day-to-day variations, but the mode peaks (C_1 and C_2) show day-to-day changes. It is therefore reasonable to use a peak ratio γ (defined as C_2/C_1 in equation (1)) to describe observed variations in aerosol size distribution. The mode peak ratio γ, which quantifies the relative abundance of two modes, has also been used for aerosol retrievals from satellites [e.g., *Mishchenko et al.*, 1999; *Higurashi and Nakajima*, 1999]. *Higurashi and Nakajima* [1999] (hereinafter referred to as HN99) and *Mishchenko et al.* [1999] used a bilognormal size distribution with r_{v1} of 0.17 μm and r_{v2} of 3.14 μm in their two-channel AVHRR global aerosol retrieval algorithms, and showed a polynomial relationship between γ and α. Both studies [*Mishchenko et al.*, 1999; HN99] show that the relationship between γ and α can be established through Mie calculations if the parameters of two size mode (e.g., r_i and σ_i) and refractive indices are known.

[14] The refractive index is highly variable depending on the chemical compositions of aerosols [*d'Almeida et al.*, 1991]. Large differences in reported aerosol refractive indices also exist even for the same type of aerosol, for example dust [*d'Almeida*, 1987; *Sokolik et al.*, 1993; *Kaufman et al.*, 2001]. The aerosols in the study area are complex and are generally a mixture of several types of aerosols including sulfate, dust, sea salt and soot [*Higurashi and Nakajima*, 2002]. However the one-channel satellite retrieval algorithms characterize the column aerosol properties using a fixed effective refractive index [*Rao et al.*, 1989; *Ignatov et al.*, 1995; *Wagener et al.*, 1997; *Zhang et al.*, 2001; *Christopher and Zhang*, 2002; *Wang et al.*, 2003]. (Effective refractive index does not refer to any specific aerosol type, but is suitable to quantify the composite radiative properties of all aerosols in an atmospheric column.) While the real part of the effective refractive index (i.e., 1.50–1.55) is consistent in the reported literature, the imaginary component of refractive index shows large variations. For example, the imaginary component of the refractive index at AVHRR ch1 wavelength (0.6 μm) varies from nonabsorbing [*Rao et al.*, 1989; *Wagener et al.*, 1997] to values considered absorbing 0.003–0.005i [*Geogdzhayev et al.*, 2002; *Mishchenko et al.*, 1999; HN99]. Recently a survey of aerosol properties from worldwide AERONET sites implied that the imaginary part of the refractive index of desert dust and oceanic aerosols range from 0.0015 to 0.0007 and the single scattering albedo varied from 0.95 to 0.98 at 0.67 μm [*Dubovik et al.*, 2002]. Those single scattering values derived from Sun and sky measurements using a robust inversion technique [*Dubovik et al.*, 2000; *Dubovik and King*, 2000], represent the effective aerosol properties in the atmospheric column and are suitable for satellite remote sensing retrievals algorithms. *Dubovik et al.* [2002] found that dust aerosols have similar real part of refractive index when compared to values reported by *Patterson et al.* [1977] for dust, while the imaginary part of refractive index was smaller, more consistent with the analysis of *Kaufman et al* [2001]. Although there is expected to be some amount of soot loading in our study area [*Higurashi and Nakajima*, 2002], the soot content and its effect on the column aerosol properties is still unknown. Therefore in this study, we use the real part of refractive index from *Patterson et al.* [1977] but reduce the imaginary part refractive index by 70% to be consistent with AERONET retrievals [*Dubovik et al.*, 2002]. We use the wavelength-dependent refractive index from *Patterson et al.* [1977] in the radiative transfer model calculation to create the LUT (section 3.2). The refractive index used in this study at 0.67 μm is 1.53–0.002i.

[15] Using the above refractive index and the derived bilognormal distribution, we establish the relationship between α and γ through Mie calculations (Figure 3). Also shown in Figure 3 is the single scattering albedo (ω_0) as a function of γ and the values used by [cf. HN99, Figure 3]. For the same γ, the ω_0 values in the east Asian regions are larger than those in HN99 mainly because of the difference in the imaginary part of the refractive index (0.002i versus 0.005i). Using Figure 3, the Ångström exponent α can be used to derive γ, which can then be used together with derived size distribution mode parameters and refractive indices in Mie calculations to infer aerosol optical properties. In the HN99 global retrieval algorithms, the pair of (τ, α) is simultaneously retrieved from the two channel AVHRR algorithm by using a LUT in which TOA reflectance is a function of θ_0, θ, ϕ, ρ_0, τ, α. In this study, similar calculations are performed using a discrete ordinate radiative transfer model [*Ricchiazzi et al.*, 1998] to create the LUT. However, since the GMS5 only has one visible

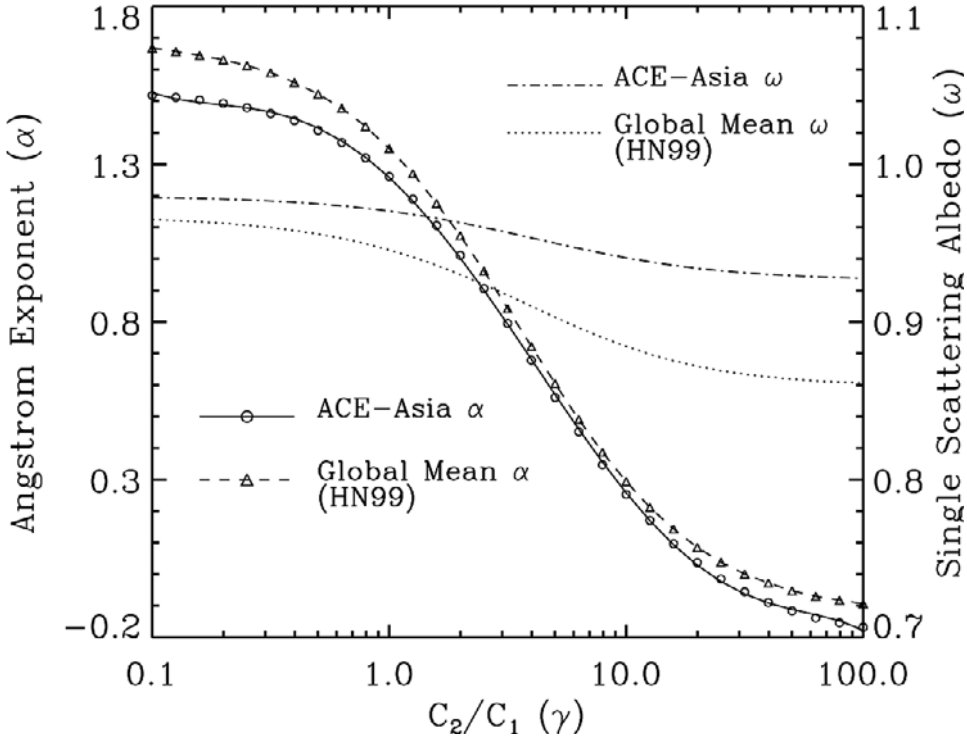

Figure 3. The Ångström exponent and single scattering albedo as a function of peak ratio of bimodal size distribution in ACE-Asia and the comparison with global mean [*Higurashi and Nakajima*, 1999].

channel, the (τ, α) pair cannot be retrieved simultaneously. Therefore, for each GMS5 pixel, the α values must be calculated from other sources. To achieve this, a successive correction method (SCM) is used to dynamically infer α from the ship, AERONET, and aircraft measurements (Appendix A). The SCM [*Koch et al.*, 1983] is a relatively simple and widely used interpolation method that merges irregular point data from observation sites onto regular grids (Appendix A). In this study, we use this method to interpolate the Ångström exponent α inferred from the ground measurements (e.g., Sun photometers at different AERONET sites, Figure 1), ship measurement (e.g., Sun photometer on board NOAA R/V *Ron Brown*) and aircraft measurements (e.g., AATS6 on board C-130 and AATS14 on Twin Otter) into regularly spaced grids in the study area.

3.2. Retrieval Method

[16] The retrieval process has three major steps. Using the SCM technique, the first step is to create the daily spatial distribution of the Ångström exponent in the study region using ship, AERONET and aircraft measurements (Appendix A). The second step is to generate a background (clear sky) reflectance map and detect aerosols over the study area. Then the Ångström exponent is obtained for each aerosol pixel as identified by the GMS imager from step 1. The α value is then used to retrieve the AOT of each aerosol pixel from the previously computed LUT.

[17] This study uses the technique described in the work of *Wang et al.* [2003] to derive the background ocean reflectance and to detect aerosol pixels. Using a minimum composite method, the spatial distribution of background or "clear sky" reflectance is obtained for each hourly GMS5 observation time [*Wang et al.*, 2003; *Zhang et al.*, 2001; *Moulin et al.*, 1997]. Cloudy pixels are judged based on the IR temperature, spatial coherence (standard deviation) of the 3×3 pixel array in ch2 and ch3 images and the contrast of diurnal temperature (from infrared channels, ch2, and ch3) [*Wang et al.*, 2003]. To further reduce cloud contamination, the spatial coherence of the 3×3 pixel array in ch1 images is used. Further details of this method can be found in the work of *Wang et al* [2003]. At this stage, for each aerosol pixel, the α value is available from the computed spatial distribution of Ångström exponent (Appendix A). The AOT is retrieved by finding the best match between the satellite reflectance and precalculated reflectance from the LUTs which is a function of θ_0, θ, ϕ, ρ_0, τ, α.

4. Results

[18] In this section, we first present the monthly mean distribution of GMS5 retrieved AOT during April 2001 (Figure 4a), followed by detailed analysis of the retrieval results and the comparison with ground and in situ AOT measurements. The monthly mean GMS5 AOT map (Figure 4a) demonstrates the transport pattern of aerosols with high AOT near the coast of east China and low AOT over the open ocean. The monthly mean AOT in the study area (Figure 4a) is 0.33. There are two distinct aerosol features, as illustrated in Figure 4a, one from the northern coast of China (37°N, 125°E) extending to Korea and another from the eastern coast of China (32°N, 125°E) extending to southern Japan. This is consistent with previous studies [*Prospero et al.*, 2002; *Chun et al.*, 2001b; *Murayama et al.*, 2001; *Husar et al.*, 2001; *Zhou et al.*, 2002] which showed that depending on meteorological conditions, the dust aerosols from northwest China can be transported either to Korea or further south

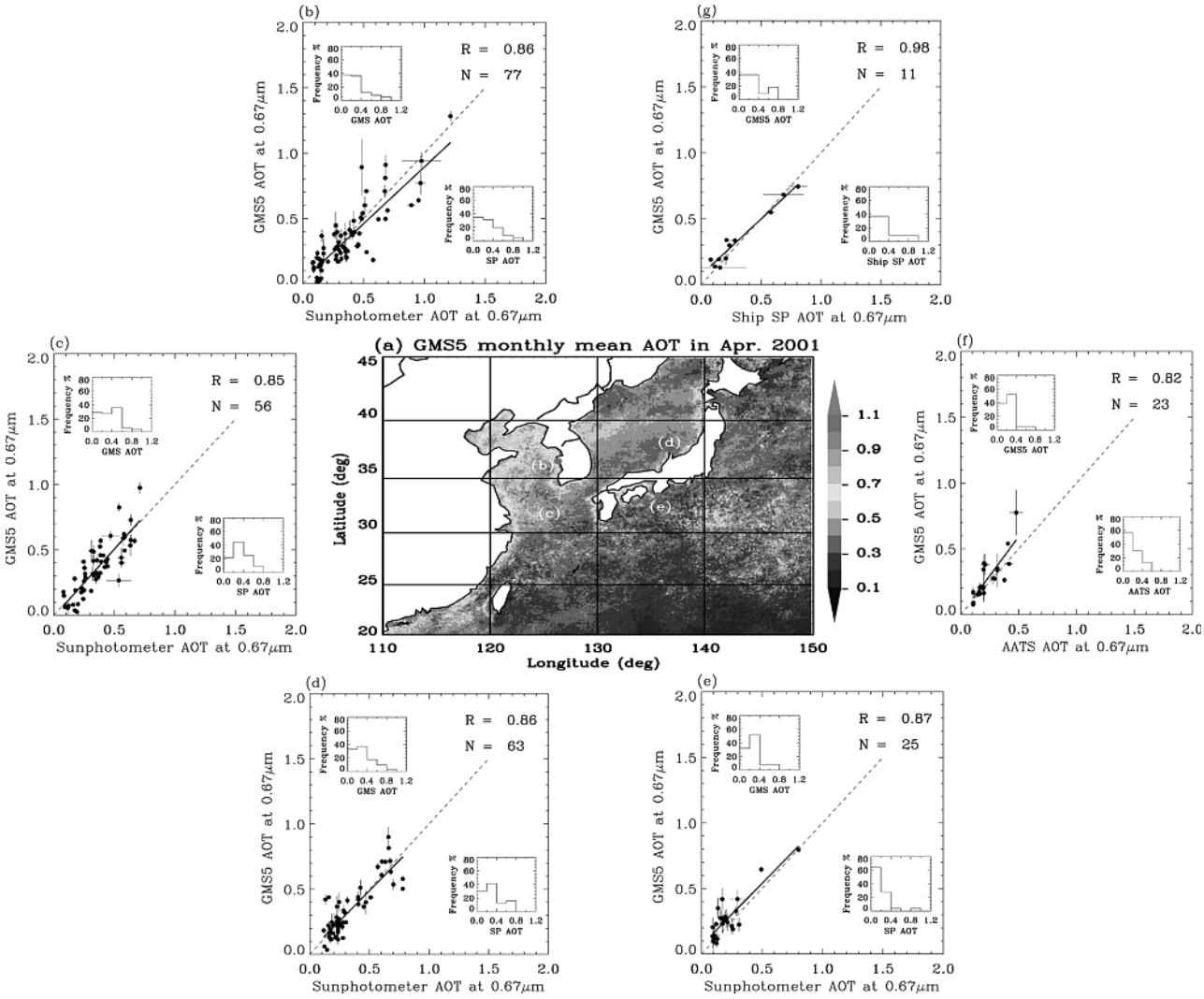

Figure 4. (a) Monthly mean GMS5 AOT and the comparison of GMS5 AOT with the AOT inferred from SP at (b) Anmyon and (c) Cheju, (d) Noto and (e) Shirahama as well as AOT inferred from (f) AATS6 and AATS14 and (g) ship SP. Letters b–e in Figure 4a shows the location of four AERONET sites Anmyon, Cheju, Noto, and Shirahama, respectively. Dotted line is the one-to-one correspondence and the solid line is the best fit to the points. See color version of this figure at back of this issue.

(e.g., Yangze River, around 30°N), moving eastward to southern Japan. Note that the GMS5 retrievals in this study show a coastal effect, which is due to the high surface reflectance near the coastal areas. This effect is also apparent in other retrievals such as AVHRR [*Husar et al.*, 1997], and GOES8 [*Wang et al.*, 2003]. The retrieval uncertainty due to surface reflectance is discussed in section 5.

[19] To validate the satellite retrievals, we compared the GMS retrievals with the AOT inferred from AERONET, ship and aircraft measurements. While the Sun photometer measures the direct solar irradiance at specific wavelengths with narrow fields of view to infer the aerosols optical thickness, the satellite imager measures the upwelling radiance at larger spatial resolutions. Several papers have discussed the difference between the satellite and AERONET measurements and have proposed different methods for comparing the two data sets [*Zhao et al.*, 2002; *Ichoku et al.*, 2002; *Zhang et al.*, 2001; *Wang et al.*, 2003]. The basic procedure is to use spatial quantities from satellite retrievals (e.g, mean and standard deviation) and compare them with the temporal variation of Sun photometer measurements. The size of the spatiotemporal window can be carefully chosen so that the difference due to high temporal and spatial variations can be minimized. A spatial window of 9×9 GMS5 pixels was chosen over the ocean area nearest to each ground Sun photometer along the east-west direction. To avoid coastal effects, the spatial window is 3 pixels away from the each Sun photometer site [*Wang et al.*, 2003; *Tanré et al.*, 1997]. The temporal window of the Sun photometer measurements is ±30 min centered at each GMS observation time period to correspond with the hourly GMS data. On the basis of TOMS data, *Ichoku et al.* [2002] showed that the speed of an aerosol front is on the order of 50 km h^{-1}. Hence the size of the chosen GMS5 spatial window in this study (i.e., 9×9 GMS pixels, about 45×45 km) is consistent with other studies [e.g., *Ichoku et al.*, 2002].

[20] Figures 4b, 4c, 4d, and 4e shows the comparisons between the GMS and AERONET aerosol optical thickness

Table 3. Statistics of the Comparison Between GMS5 AOT and AERONET AOT for Four Locations[a]

Station/Instrument	N_{cp}/N_{tp}	N_{sp}/N_{tsp}	R	Linear Fit Equation	SP, $\mu \pm \sigma$	GMS, $\mu \pm \sigma$	RMSE	Bias
Anmyon	77/117	241/363	0.86	Y = 0.87X + 0.03	0.35 ± 0.24	0.33 ± 0.24	0.12	−0.02
Cheju	56/86	213/315	0.85	Y = 1.03X−0.01	0.35 ± 0.17	0.35 ± 0.20	0.10	0.0
Noto	63/87	188/268	0.86	Y = 0.93X + 0.02	0.32 ± 0.19	0.32 ± 0.19	0.09	0.0
Shirahama	25/36	113/153	0.87	Y = 0.94X + 0.07	0.21 ± 0.15	0.26 ± 0.16	0.09	0.05
AATS[b]	23/24	4135/4193	0.82	Y = 1.19X + 0.0	0.23 ± 0.11	0.27 ± 015	0.10	0.04
Ship	11/11	86/86	0.98	Y = 0.85X + 0.07	0.32 ± 0.25	0.34 ± 0.21	0.06	0.03

[a] N_{tp} and N_{cp} denote total collocated GMS and AERONET pairs within the temporal-spatio criteria window (see text), and the actual pairs used in the comparison, respectively. Owing to the differences between Sun photometer and GMS retrieval algorithms and spatial resolutions, there are cases where SP reported AOT values whereas the GMS identified these points as being cloud-contaminated. N_{tsp} and N_{sp} denote total and actual number of AERONET points used in the comparison. Note that there could be several SP points within one hour that is used to create this value. The mean and standard deviation ($\mu \pm \sigma$), root mean square error (RMSE) and bias (mean of GMS-AERONET AOT) as well as linear fit equation and linear correlation coefficient (R) between GMS and AERONET AOT are also shown.

[b] AATS includes AATS6 and AATS14.

at four locations and relevant statistics are shown in Table 3. There is good agreement between the AOT values derived from GMS and Sun photometer measurements, although the best fit line is not the same for different locations. As an example, GMS AOT retrievals underestimate AERONET AOTs at Anmyon by 0.02 (Figure 4b and Table 3), but overestimate the SP AOTs at Shirahama by 0.05 (Figure 4e and Table 3). This is possibly due to high spatiotemporal variations of aerosol properties as well as the uncertainties in the retrieval algorithms (section 5). Figure 4 also shows that large discrepancies between GMS AOT and AERONET AOT are always accompanied by large spatial and temporal variations of AOTs, demonstrating that subpixel cloud contamination and the complexity (e.g., inhomogeneity) of aerosol properties within the GMS window (e.g., about 45 km × 45 km) is possible. Nevertheless, Figure 4 and Table 3 shows that there are no systematic errors in the GMS5 retrievals, implying that both the surface reflectance and aerosol optical properties are well characterized in retrieval algorithms. However, further improvement would be possible if the spatial and radiometric resolution of GMS5 were increased and more observation data points could be obtained for derivation of the spatial distribution of the Ångström exponent. Overall, the mean root mean square error (RMSE) of the AOTs from the GMS retrievals are within 0.1, and the differences between GMS aerosol optical thickness and the collocated AERONET values for the entire month are within 0.05 (see the last column of Table 3).

[21] Figures 4f and 4g shows the AOT comparisons between the GMS5 and AATS6/AATS14 and ship measurements, respectively. The GMS5 AOT is a column value, while the AATS6 and AATS14 emphasize measurements of aerosol profiles. Comparison is only made on days when the AATS6/AATS14 profiles are available over the ocean; less than 100 m above the surface and within ±30 min of GMS5 observation times. The GMS5 has a temporal resolution of one hour, while the AATS6/AATS14 can measure AOT at much higher temporal resolution (on the order of minutes), the spatial quantities from satellite retrievals (e.g, mean and standard deviation) are used to compare the temporal quantities of AATS6/AATS14 AOT. In each comparison, we first calculate the range of a GMS5 box that bounds the AATS route in one hour. The mean and standard deviation of the GMS5 AOTs in that box is used for the comparison. Depending on the flight, the size of the box may vary. Totally twenty four pairs of intercomparison data between GMS5 and AATS6/AATS14 are found; only 23 pairs are used because the GMS5 classified one point as being cloud contaminated. The AATS6 does not have a wavelength centered 0.67 μm, therefore the AATS6 AOT at this wavelength is derived by fitting the Ångström AOT wavelength-dependent relationship [*Redemann et al.*, 2003] ($\tau_{\lambda_1} = \tau_{\lambda_2}(\lambda_1/\lambda_2)^{-\alpha}$, where τ_{λ_1}, τ_{λ_2} are AOT values at λ_1, λ_2, respectively, and α is Ångström exponent). The relevant statistics are shown in the last row of Table 3. When compared to the AERONET measurements, the AOT inferred from aircraft and ship measurements are less influenced by coastal effects and therefore they are important to estimate the robustness of the satellite retrieval algorithms. As shown in Figures 4f and 4g, there is good agreement between GMS5 AOT and ship inferred AOT as well as aircraft values except for one point in Figure 4e where both GMS5 AOT and AATS AOT show relatively large variations. Since GMS5 has a pixel resolution of 5 × 5 km^2, its retrieval accuracy will be decreased if there is a subpixel cloud and the large subpixel variations of aerosol distributions and properties.

[22] Several studies have shown that aerosols could have large diurnal variations on the timescale of hours, especially during an aerosol episode [*Levin et al.*, 1980; *Christopher et al.*, 2003; *Wang et al.*, 2003]. In this section, we examine the potential of GMS5 to estimate the daytime diurnal variation of AOT. To illustrate the time sequence of diurnal change of AOT over the four Sun photometer locations, we chose a typical aerosol event at each observation site (Figure 5). Figure 5 shows that GMS5 AOT can generally capture the peak values of aerosol AOT during the aerosol event and can describe the phase of AOT diurnal changes during the GMS5 observation time period. The largest change is found at the Anmyon site, which is not surprising since this site is nearest to the Asian continent. The AOT at the Anmyon site on 23 April 2001 was about 0.2; increased to 0.5 on the next day, and increased further to 1.2 on 25 April 2001. The dust layer passed the Anmyon site on 25 April and AOT decreased to 0.2 on 26 April. This event is well documented by the GMS5 retrievals during the available observation time period. Without the high temporal resolution of geostationary instruments, these peak values may not be captured by satellite instruments that obtain measurements only at one time of the day. However, there are also several points where the GMS5 did not capture the peak AOT, although the daily mean AOT matches the SP AOT values (e.g., 10–11 April 2001 at Noto). The next generation of geostationary imagers (e.g., Meteosat Second Generation

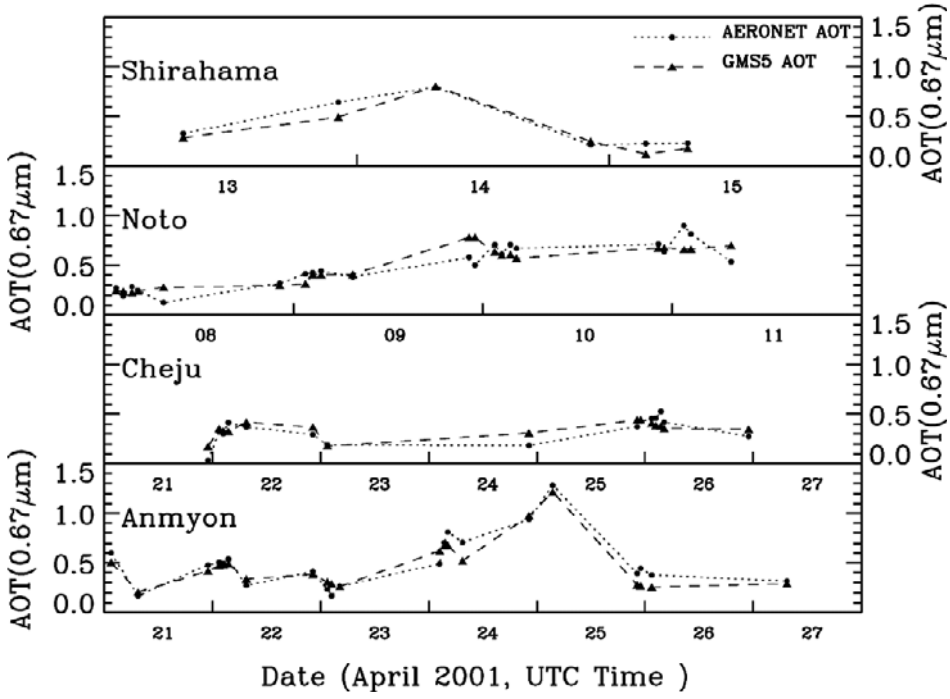

Figure 5. A time sequence of SP AOT and GMS-5 AOT in different AERONET sites for selected days when large diurnal change accompanying dust event occurred.

(MSG) [*Schmetz et al.*, 2002]) with improved spectral, spatial and radiometric resolutions along with an increased number of visible channels will significantly improve the accuracy of aerosol retrievals.

5. Uncertainty Analysis

[23] The key sources of uncertainty can be divided into four categories, including surface conditions, aerosol models, aerosol detection method, and sensor calibration. Compared to land surfaces, the ocean is relatively dark and homogeneous. *Wang et al.* [2003] discuss the variations of ocean surface reflectance due to several factors such as near surface ocean wind speed and its consequent white cap effects, the residual Sun glint contamination effect, the chlorophyll content and high turbulence coastal waters, and found that that the overall variations in surface reflectance is relatively small, about 0.2%–0.4% under normal conditions (i.e., wind speed about 7 ms^{-1}) and could be large as 1% in some extreme conditions (e.g., sea wind speed higher than 15 ms^{-1}). In this study, we found that a 0.2%–0.4% change in surface reflectance (ρ_0) will result in an average uncertainty of 0.01–0.03 in AOT retrievals.

[24] The GMS5 was launched on 18 March 1995. The visible channel of the GMS VISSR imager does not have an onboard calibration. Geostationary satellites typically undergo degradation during the operation period due to the accumulation of materials on the scanning mirror [*Ellrod et al.*, 1998]. The sensor calibration is very important for the retrievals of accurate AOTs [*Wang et al.*, 2003; *Zhang et al.*, 2001; *Geogdzhayev et al.*, 2002]. We first evaluate the ability of VISSR to detect aerosols in terms of the sensor detection limit, defined as the minimal AOT (τ) required to produce an increment of one digital count (DC) for non-cloudy areas over an ocean background (i.e., $d\tau/d$DC) [*Wang et al.*, 2003; *Moulin et al.*, 1997], and then examine the AOT retrieval uncertainty due to GMS5 calibrations. Figure 6 shows the collocated GMS5 S-VISSR digital count (in 8 bits) versus collocated SP AOT at 0732 UTC (θ_0 = 51 and θ = 31) during different days at Cheju, Gosan. Compared to other AERONET sites during ACE-Asia IOP, Cheju is a small island isolated from the continent, with a relatively homogenous dark background. Hence it provides an ideal place to evaluate the aerosol signature on the GMS5 image. Figure 6 shows a positive correlation between AOT

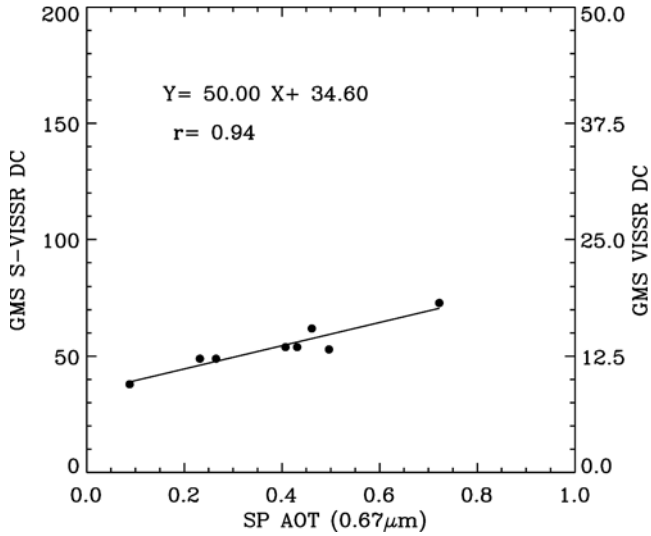

Figure 6. Scatterplot of GMS S-VISSR digital count (DC) versus collocated SP AOT over Cheju AERONET site at 0732 UTC during different days. Right side shows the corresponding VISSR digital count (in 6 bits) (SZA = 51, VZA = 31).

and the GMS5 S-VISSR digital count, with a linear coefficient of 0.94 and a best fit equation:

$$DC = 50\tau + 34.6, \quad \frac{d\tau}{dDC} = 0.02. \tag{2}$$

[25] It is important to note that the digital count (8 bits) of S-VISSR used in this study has been stretched from VISSR raw digital count (6 bits). Hence, based on equation (2), we estimated that the VISSR aerosol detection limit is 0.08, which is larger than that of GOES8 (0.043) [*Wang et al.*, 2003] and similar to that of Meteosat2 (0.06) [*Moulin et al.*, 1997]. In other words, GOES8 is better suited for aerosol detection due to the higher radiometric resolution (10 bits) compared to GMS5 (6 bits) and Meteosat2 (6 bits). METEOSAT4 and METEOSAT5 have 8 bits radiometric resolution and consequently have a lower detection limit (less than 0.06) [*Moulin et al.*, 1997]. However, with the stretched technique, S-VISSR data might enhance the aerosol signature and could have a detection limit similar to GOES8. We emphasize that this is only an approximate analysis, and the conclusions may be affected by other factors such as the aerosol single scattering albedo and phase function [*Knapp and Vonder Haar*, 2000].

[26] In this study, the ISCCP calibration coefficients are used for converting the GMS5 digital counts to reflectance. The calibration coefficients are derived by comparing GMS5 and polar orbiting satellites with the same viewing geometry for coincident scenes such as homogenous cloud over the ocean and bright desert [*Desormeaux et al.*, 1993]. This procedure was recently refined to reduce the artifacts in the calibrations associated with the changes in the polar orbiting satellite orbits as well as localized anomalies related to occasional errors in the geostationary satellites [*Brest et al.*, 1997]. The uncertainty of the ISCCP absolute calibration for visible channel is within 10% [*Brest et al.*, 1997]. There are several studies that proposed different methods to vicariously calibrate the geostationary satellites [e.g., *Marshall et al.*, 1999; *Fraser and Kaufman*, 1985; *Moulin et al.*, 1996]. However, direct comparison among these studies is difficult due to the different sensors and different time periods examined. Nevertheless, if the calibration uncertainty is within 10%, our calculations show there will be an uncertainty of 10% in the AOT retrievals. The monthly mean AOT value at 0.67 μm varies in different AERONET sites (see Table 3) from 0.23 to 0.35, therefore we estimate that for an upper limit in AOT of 0.5, the uncertainty will be less than 0.05.

[27] In this study, the aerosol optical properties are characterized by using a dynamical model in which both the aerosol size distribution and the Ångström exponent are inferred from observations. Hence the major uncertainty in this dynamical model is from the assumed aerosol refractive indices and the derived α values. As shown in Appendix A, the uncertainty in α calculated from the SCM method is within 0.15. Figure 7 shows the simulated TOA reflectance as a function of α and AOT for a given solar zenith angle ($\theta_0 = 40°$), viewing zenith angle ($\theta = 40°$), relative azimuth angle ($\phi = 80°$) and surface reflectance ($\rho_0 = 0.04$). Figure 7 shows different pairs of (AOT, α) may have the same effect (e.g., same reflectance) at the top of atmosphere. The contour of TOA reflectance is skewed toward the larger

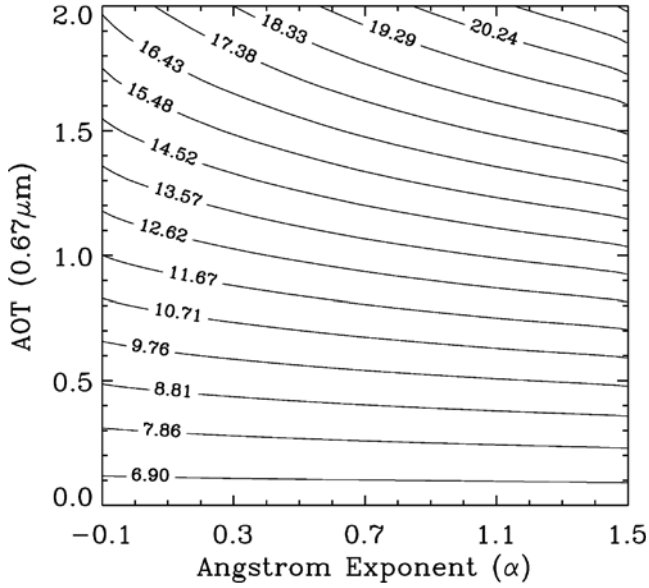

Figure 7. Contour plot of simulated TOA reflectance (%) as a function of AOT and Ångström from exponent for solar zenith angle ($\theta_0 = 40°$), viewing zenith angle ($\theta = 40°$), relative azimuth angle $\phi = 80^o$) and surface reflectance ($\rho_0 = 0.04$).

AOT (positive *y* axis direction) when α decreases, implying that the decrease of α, hence the decrease of single scattering albedo (cf. Figure 3), can be compensated by an increase of AOT, resulting in the same TOA reflectance. Therefore, for a GMS5 pixel with a specific reflectance, the slope (dAOT/$d\alpha$) in Figure 7 actually describes how the AOT retrievals change due to a change in α value. On the basis of Figure 7, dAOT/$d\alpha$ is small (<0.1) for $\alpha > 0.3$ and AOT < 0.5, and becomes larger when AOT becomes larger and α becomes smaller. dAOT/$d\alpha$ could be as large as 0.3 (cf. contour line of 16.43) in Figure 7. We conclude that the dAOT/$d\alpha$ is smaller than 0.1 during the retrievals as most pixels have an AOT smaller than 0.5 (cf., Table 3). Hence a change of 0.15 in the Ångström exponent will result in an uncertainty of about 0.02 in AOT retrievals.

[28] To evaluate the effect of the imaginary part of refractive index (*Ri*) on retrievals, we changed the assumed R_i value of 0.002 from 0.004 to zero, while keeping other parameters the same to recreate the LUT. Our calculations show that AOT would increase by 0.04 if R_i decreases by 0.002. A change in R_i from 0.004 to zero leads to a change in single scattering albedo from −0.02 to 0.02 for different size ratios γ (cf. Figure 3). If we define the sensitivity of the retrieved AOT (τ) to R_i as $(\Delta\tau/\tau)/(\Delta Ri/Ri)$ [*Wang et al.*, 2003], we find that the sensitivity could be 40% for τ less than 0.1 and 8% for τ around 0.5, implying that the uncertainty in AOT associated with the imaginary part of refractive index might result in significant retrieval errors in situations with low aerosol loadings [*Wang et al.*, 2003; *Mishchenko et al.*, 1999]. We estimate that the uncertainty in retrievals due to uncertainties in the imaginary part of the refractive index is within 0.05.

[29] Through the analysis above, we conclude that the average uncertainty in our retrievals of AOT is about 0.08

with a maximum uncertainty of 0.15 mainly due to the assumptions in calibration (±0.05), surface reflectance (±0.01–±0.03), imaginary part of the refractive index R_i (±0.05) and assumptions in the dynamic aerosol model (±0.02). These uncertainties could also offset each other [*Wagener et al.*, 1997; *Mishchenko et al.*, 1999; *Ignatov et al.*, 1995], thereby making it a challenge to define one specific uncertainty value for the comparison between satellite retrievals and ground/in situ measurements.

6. Summary and Conclusions

[30] Using bilognormal size distributions inferred from measurements during ACE-Asia in April 2001, and a refractive index value of 1.53–0.002i at 0.67 μm in Mie calculations, a relationship between Ångström exponent (α) and mode ratio (γ) is first established. A look-up table is then constructed by using Mie results in the DISORT calculations for different pairs of AOT (τ) and Ångström exponent (α). Using Sun photometer measurements from 12 AERONET sites, aircraft measurements (AATS6/AATS14) and a Sun photometer on a ship, the spatial distribution of Ångström exponent with a resolution of 2.5° × 2.5° in latitude-longitude is created. During retrievals, the Ångström exponent (α) of each GMS5 pixel was dynamically defined using a daily Ångström map. The AOT of a given GMS5 pixel is then calculated by fitting the GMS5 reflectance with the simulated TOA reflectance. Our results show there is good agreement between GMS5 retrievals and AOT measured by Sun photometer on the ship (with linear coefficient R = 0.98), AATS6/14 on aircraft (R = 0.82) and the Sun photometers from four AERONET sites (R = 0.86, 0.85, 0.86 0.87 for Anmyon, Cheju, Noto and Shiraham, respectively). Our uncertainty analysis shows that the average uncertainty in satellite retrievals is about 0.08 with maximum of 0.15 mainly due to assumptions in calibration (±0.05), surface (±0.01–±0.03), imaginary part of refractive index *Ri* (±0.05) and the dynamic aerosol model (±0.02). These results indicate that geostationary satellite retrievals play a complementary role to polar orbiting retrievals and can provide critical information on the diurnal variation of aerosols.

[31] In summary we emphasize that the retrieval algorithms developed in this study are built upon intensive ground and aircraft observations during the ACE-Asia IOP. Although ground and aircraft observations usually are accurate they are limited in space and time. Therefore using ground and aircraft information in satellite retrievals is a necessary step to improve retrievals and estimations of aerosol forcing. For this purpose, the Ångström exponent inferred from in situ and ground observations were used in the retrieved algorithms. However, caution must be exercised in situations where the Ångström exponent cannot be reliably inferred. The good agreement between GMS5 and Sun photometer inferred AOT in this study implies the usefulness of this approach and good utilization of valuable information in ground and aircraft observations. With more visible channels in the next generation of geostationary imagers such as MSG [*Schmetz et al.*, 2002], both Ångström factor and AOT can be retrieved simultaneously. Hence it is expected that the next generation of geostationary imagers will significantly improve our capability to monitor aerosols and provide accurate estimates of the effect of aerosols on the radiation balance of the Earth-atmosphere system.

Appendix A: Application of the Successive Correction Method (SCM)

[32] The SCM method was originally designed to interpolate the normal meteorological data in irregularly located observation sites onto the regular grid points that can be used in numerical models [*Koch et al.*, 1983]. In this study, we use this method to interpolate the Ångström exponent α inferred from the ground measurements (e.g., SP at different AERONET sites, Figure 1), ship measurement (e.g., SP on board NOAA R/V *Ron Brown*) and aircraft measurements (e.g., AATS6 on board C-130 and AATS14 on Twin Otter) into regularly spaced grids in the study area. The study area (Figure 1) is first segmented into 14 × 12 grids with a resolution of 2.5° × 2.5°. The α value at each grid is calculated using the following equation [*Koch et al.*, 1983]:

$$\alpha_i^0 = \alpha_i^b \quad , \quad \alpha_i^{n+1} = \alpha_i^n + \frac{\sum_{k=1}^{K} w_{ik}^n \left(\alpha_k^0 - \alpha_k^n\right)}{\sum_{k=1}^{K} w_{ik}^n}, \tag{A1}$$

where subscript i and k represents the grid point and observation site, respectively. K denotes total number of observation sites. α_i^b is the background (first guess) value at i; α_i^n is the n-th iteration estimate at i; α_k^0 is the observation at k; α_k^n is the nth iteration value at observation site k; w_{ik}^n is the weight of observation point k to the grid point i:

$$w_{ik} = \exp\left(-\frac{r_{ik}^2}{2R_n^2}\right), \tag{A2}$$

where r_{ik} is the distance between i and k; R_n is the radius of influence which is changed in each iteration by $R_{n+1}^2 = \beta R_n^2$. By choosing proper values of β and R_0, only 2–4 iterations are needed to converge $|\alpha_i^n - \alpha_i^{n+1}|$ to the desired accuracy. The background value (α_i^b) is assumed to be the same as the monthly mean α at the nearest AERONET site. The α_k^n can be estimated from four surrounding grid points α_i^n before the n + 1 iteration starts [*Koch et al.*, 1983]. On the basis of equation (A1), by assuming the daily mean α inferred from each AERONET site as α_k^0, the daily map of α with a spatial resolution 2.5° × 2.5° can be produced. To incorporate the information from aircraft and the ship measurements, the data are first mapped to the 2.5° × 2.5° grid box, and the daily mean α is calculated from the data points on the grid. The number (k) and locations of α_k^0 is changeable depending on the operations of ship and aircraft in each day.

[33] There are several methods for measuring the accuracy of the SCM method. In the first method, the field-averaged root mean square difference (rmsd) between the interpolated and observed values can be compared [*Koch et al.*, 1983]. In the second method, several observation points are first selected as validation points and are not used in the iterations

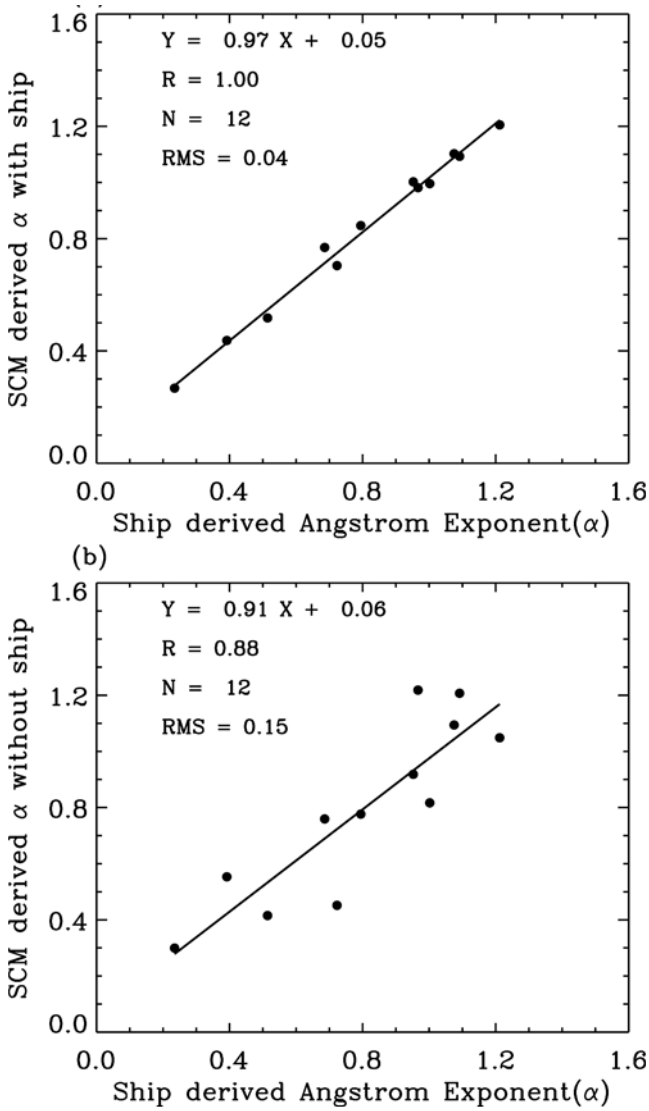

Figure A1. The comparison of ship derived Ångström exponent (x axis) with SCM derived Ångström exponent (y axis) (a) with use of ship measurements (b) without use of ship measurements during the iteration. Also shown is the best fit line, correlation coefficients (R), number of comparison points (N) and root mean square (RMS) values.

(for instance, ship measurements). Comparison is made between the final iteration results with those validation points to judge the accuracy of SCM method. This study tested both methods. The comparison of α inferred from the ship measurements with the derived values from the SCM method in both conditions, with and without use of ship measurement, is shown in Figures A1a and A1b, respectively. While Figure A1 shows the stability of the SCM, Figure A1b shows the relative accuracy of SCM. The derived and observed α generally agrees very well within the accuracy of 0.15 (Figure A1b). It is important to note that we only consider the mean value and neglect the diurnal variability of α in $2.5^\circ \times 2.5^\circ$ grid box during the derivation since the number of observations sites are limited.

[34] **Acknowledgments.** This research was partially supported by the Global Aerosol Climatology Project. F. Brechtel acknowledges the support for participation in ACE-Asia by the NOAA Office of Global Programs and the DOE Atmospheric Chemistry Program. We thank Gary Jedlovec for providing the GMS data. This research is a contribution to the International Global Atmospheric Chemistry (IGAC) Core Project of the International Geosphere Biosphere Program (IGBP) and is part of the IGAC Aerosol Characterization Experiments (ACE).

References

Bergin, M. H., G. R. Cass, J. Xu, C. Fang, L. M. Zeng, T. Yu, L. G. Salmon, C. S. Kiang, X. Y. Zhang, and W. L. Chameides, Aerosol radiative, physical, and chemical properties in Beijing during June 1999, *J. Geophys. Res.*, *106*, 17,969–17,980, 2001.

Boucher, O., and T. L. Anderson, GCM assessment of the sensitivity of direct climate forcing by anthropogenic sulfate aerosols to aerosol size and chemistry, *J. Geophys. Res.*, *100*, 26,117–26,134, 1995.

Brechtel, F. J., and G. Buzorius, Airborne observations of recent new particle formation over two urban areas in the U.S., *J. Aerosol Sci.*, *32*, S115–S116, 2001.

Brest, C. L., W. B. Rossow, and M. Roiter, Update of radiance calibrations for ISCCP, *J. Atmos. Oceanic Technol.*, *14*, 1091–1109, 1997.

Charlson, R. J., S. E. Schwartz, J. M. Hales, R. D. Cess, J. A. Coakley, J. E. Hansen, and D. J. Hoffman, Climate forcing by anthropogenesis aerosols, *Science*, *255*, 423–430, 1992.

Christopher, S. A., and J. Zhang, Daytime variation of shortwave direct radiative forcing of biomass burning aerosols from GOES 8 imager, *J. Atmos. Sci.*, *59*, 681–691, 2002.

Christopher, S. A., J. Wang, Q. Ji, and S.-C. Tsay, Estimation of diurnal shortwave dust aerosol radiative forcing during PRIDE, *J. Geophys. Res.*, *108*(D19), doi:10.1029/2002JD002787, in press, 2003.

Chun, Y., J. Kim, J. C. Choi, K. O. Boo, S. N. Oh, and M. Lee, Characterization number size distribution of aerosol during Asian dust period in Korea, *Atmos. Environ.*, *35*, 2715–2721, 2001a.

Chun, Y., K.-O. Boo, J. Kim, S.-U. Park, and M. Lee, Synopsis, transport, and physical characteristics of Asian dust in Korea, *J. Geophys. Res.*, *106*, 18,461–18,469, 2001b.

Chylek, P., and J. Wong, Effect of absorbing aerosols on global radiation budget, *Geophys. Res. Lett.*, *22*, 929–931, 1995.

d'Almeida, G. A., On the variability of desert aerosol radiative characteristics, *J. Geophys. Res.*, *92*, 3017–3026, 1987.

d'Almeida, G. A., P. Koepke, and E. P. Shettle, *Atmospheric Climatology and Radiative Characteristics*, 561 pp., A. Deepak, Hampton, Va., 1991.

Desormeaux, Y., W. B. Rossow, C. L. Brest, and C. G. Campbell, Normalization and calibration of geostationary satellite radiances for ISCCP, *J. Atmos. Oceanic Technol.*, *10*, 304–325, 1993.

Deuze, J. L., M. Herman, P. Boloub, and D. Tanré, Characterization of aerosols over ocean from POLDER/ADEOS-1, *Geophys. Res. Lett.*, *26*, 1421–1424, 1999.

Dubovik, O., and M. King, A flexible inversion algorithms for retrieval of aerosol optical properties from Sun and sky radiance measurements, *J. Geophys. Res.*, *105*, 20,673–20,696, 2000.

Dubovik, O., A. Smirnov, B. N. Holben, M. D. King, Y. J. Kaufman, T. F. Eck, and I. Slutsker, Accuracy assessments of aerosol optical properties retrieved from Aerosol Robotic Network (AERONET) Sun and sky radiance measurements, *J. Geophys. Res.*, *105*, 9791–9806, 2000.

Dubovik, O., B. Holben, T. F. Eck, A. Smirnov, Y. J. Kaufman, M. D. King, D. Tanré, and I. Slutsker, Variability of absorption and optical properties of key aerosol types observed in wordwide locations, *J. Atmos. Sci.*, *59*, 590–608, 2002.

Ellrod, G. P., R. V. Achutunl, J. M. Daniels, E. M. Prints, and J. P. N. III, An assessment of GOES-8 imager data quality, *Bull. Am. Meteorol. Soc.*, *79*, 2509–2526, 1998.

Fraser, R. S., and Y. J. Kaufman, Calibration of satellite sensors after launch, *Appl. Optics*, *25*, 1177–1185, 1985.

Geogdzhayev, I. V., M. I. Mishchenko, W. B. Rossow, B. Cairns, and A. A. Lacis, Global two-channel AVHRR retrievals of aerosol properties over the ocean for the period of NOAA-9 observations and preliminary retrievals using NOAA-7 and NOAA-11 data, *J. Atmos. Sci.*, *59*, 262–278, 2002.

Hansen, J., M. Sato, and R. Ruedy, Radiative forcing and climate response, *J. Geophys. Res.*, *102*, 6831–6864, 1997.

Herman, J. R., P. K. Bhartia, O. Torres, C. Hsu, C. Seftor, and E. Celarier, Global distribution of UV-absorbing aerosols from Nimbus 7/TOMS data, *J. Geophys. Res.*, *102*, 16,911–16,922, 1997.

Higurashi, A., and T. Nakajima, Development of a two-channel aerosol retrieval algorithm on a global scale using NOAA AVHRR, *J. Atmos. Sci.*, *56*, 924–941, 1999.

Higurashi, A., and T. Nakajima, Detection of aerosol types over the east China Sea near Japan from four-channel satellite data, *Geophys. Res. Lett.*, *29*(17), 1836, doi:10.1029/2002GL015357, 2002.

Holben, B. N., et al., AERONET—A federated instrument network and data archive for aerosol characterization, *Remote. Sens. Environ.*, *66*, 1–16, 1998.

Houghton, J. T., et al. (Eds.), *Climate Change: The IPCC Scientific Assessment*, 362 pp., Cambridge Univ. Press, New York, 1990.

Huebert, B. J., T. Bates, P. B. Russell, G. Shi, Y. J. Kim, K. Kawamura, G. Carmichael, and T. Nakajima, An overview of ACE-Asia: Strategies for quantifying the relationships between Asian aerosols and their climatic impacts, *J. Geophys. Res.*, *108*(D23), 8633, doi:10.1029/2003JD003550, in press, 2003.

Husar, R. B., J. M. Prospero, and L. L. Stowe, Characterization of tropospheric aerosols over the oceans with the NOAA/AVHRR optical thickness operational product, *J. Geophys. Res.*, *102*, 16,889–16,909, 1997.

Husar, R. B., et al., Asian dust events of April 1998, *J. Geophys. Res.*, *106*, 18,317–18,330, 2001.

Ichoku, C., D. A. Chu, S. Chu, Y. J. Kaufman, L. A. Remer, D. Tanré, I. Slutsker, and B. N. Holben, A spatio-temporal approach for global validation and analysis of MODIS aerosol products, *Geophys. Res. Lett.*, *29*(12), 8006, doi:10.1029/2001GL013206, 2002.

Ignatov, A. M., L. L. Stowe, S. M. Sakerin, and G. K. Korotaev, Validation of the NOAA/NESDIS satellite aerosol product over the North Atlantic in 1989, *J. Geophys. Res.*, *100*, 5123–5132, 1995.

Intergovernmental Panel on Climate Change (IPCC), *Climate Change 2001, The Scientific Basis: Contribution of Working Group I to the Third Assessment Report of the Intergovernmental Panel on Climate Change*, edited by J. T. Houghton et al., 881 pp., Cambridge Univ. Press, New York, 2001.

Junge, C. E., The size distribution and aging of natural aerosols as determined from electrical and optical properties found in the marine boundary layer over the Atlantic Ocean, *J. Meteorol.*, *12*, 13–25, 1955.

Kahn, R., R. West, D. McDonald, and B. Rheingans, Sensitivity of multi-angle remote sensing observations to aerosol sphericity, *J. Geophys. Res.*, *102*, 16,861–16,870, 1997.

Kaufman, Y. J., D. Tanré, L. A. Remer, E. F. Vermote, A. Chu, and B. N. Holben, Operational remote sensing of tropospheric aerosol over land from EOS moderate resolution imaging spectroradiometer, *J. Geophys. Res.*, *102*, 17,051–17,076, 1997.

Kaufman, Y. J., D. Tanré, O. Dubovik, A. Karnieli, and L. A. Remer, Absorption of sunlight by dust as inferred from satellite and ground-based remote sensing, *J. Geophys. Lett.*, *28*, 1479–1482, 2001.

Kaufman, Y. J., D. Tanré, and O. Boucher, A satellite view of aerosols in climate systems, *Nature*, *419*, 215–223, 2002.

Kiehl, J. T., and B. P. Briegleb, The radiative roles of sulfate aerosols and greenhouse gases in climate forcing, *Science*, *260*, 311–314, 1993.

Knapp, K. R., and T. H. Vonder Haar, Calibration of the eighth Geostationary Observational Environmental Satellite (GOES-8) imager visible sensor, *J. Atmos. Oceanic Technol.*, *17*, 1639–1644, 2000.

Koch, S. E., M. Desjardins, and P. J. Kocin, An interactive Barnes objective map analysis scheme for use with satellite and conventional data, *J. Clim. Appl. Meteorol.*, *22*, 1487–1503, 1983.

Levin, Z., J. H. Joseph, and Y. Mekler, Properties of Sharav (Khamsin) dust—Comparison of optical and direct sampling data, *J. Atmos. Sci.*, *27*, 882–891, 1980.

Li, X., et al., The cooling of SiChuan Province in recent 40 years and its probable mechanisms, *Acta Meteorol. Sin.*, *9*(1), 57–68, 1995.

Liou, K. N., *An Introduction to Atmospheric Radiation*, 2nd ed., 583 pp., Academic, San Diego, Calif., 2002.

Livingston, J. M., et al., Airborne Sun photometer measurements of aerosol optical depth and columnar water vapor during the Puerto Rico Dust Experiment and comparison with land, aircraft, and satellite measurements, *J. Geophys. Res.*, *108*(D19), 8588, doi:10.1029/2002JD002520, 2003.

Luo, Y., X. Lu, X. Zhao, W. Li, and H. Qing, Characteristics of the spatial distribution and yearly variation of aerosol optical depth over China in last 30 years, *J. Geophys. Res.*, *106*, 14,501–14,513, 2001.

Marshall, F. L., J. J. Simpson, and Z. Jin, Satellite calibration using a collocated nadir observation technique: Theoretical basis and application to the GMS-5 pathfinder benchmark period, *IEEE Trans. Geosci. Remote Sens.*, *38*, 499–507, 1999.

McKendry, I. G., J. P. Hacker, R. Stull, S. Sakiyama, D. Mignacca, and K. Reid, Long-range transport of Asian dust to the Lower Fraser Valley, British Columbia, Canada, *J. Geophys. Res.*, *106*, 18,361–18,370, 2001.

Menon, S., J. Hansen, L. Nazarenko, and Y. Luo, Climate effect of black carbon aerosols in China and India, *Science*, *297*, 2250–2252, 2002.

Meterological Satellite Center (MSC), *The GMS User's Guide*, Meterol. Satell. Cent., Tokyo, 1997.

Mishchenko, M. I., J. M. Dlugach, E. G. Yanovitskij, and N. T. Zakharova, Bi-directional reflectance of flat, optically thick particulate layers: An efficient radiative transfer solution and applications to snow and soil surfaces, *J. Quant. Spectrosc. Radiat. Transfer*, *63*, 409–432, 1999.

Moulin, C., C. E. Lambert, J. Poitou, and F. Dulac, Long term (1983–1994) calibration of the Meteosat solar (VIS) channel using desert and ocean targets, *Int. J. Remote Sens.*, *17*, 1183–1200, 1996.

Moulin, C., F. Dulac, C. E. Lambert, P. Chazette, I. Jankowiak, B. Chatenet, and F. Lavenn, Long-term daily monitoring of Sahara dust load over ocean using Meteosat ISSCP-B2 data: 2. Accuracy of the method and validation using Sun photometer measurements, *J. Geophys. Res.*, *102*, 16,959–16,969, 1997.

Murayama, T., et al., Ground-based network observation of Asian dust events of April 1998 in east Asia, *J. Geophys. Res.*, *106*, 18,345–18,360, 2001.

Patterson, E. M., D. A. Gillette, and B. H. Stockton, Complex index of refraction between 300 and 700 nm for Saharan aerosols, *J. Geophys. Res.*, *82*, 3153–3160, 1977.

Prospero, J. M., P. Ginoux, O. Torres, S. E. Nicholson, and T. E. Gill, Environmental characterization of global sources of atmospheric soil dust identified with the NIMBUS 7 Total Ozone Mapping Spectrometer (TOMS) absorbing aerosol product, *Rev. Geophys.*, *40*(1), 1002, doi:10.1029/2000RG000095, 2002.

Ramanathan, V. P., J. Crutzen, J. T. Kiehl, and D. Rosenfeld, Aerosols, climate, and the hydrological cycle, *Science*, *294*, 2119–2124, 2001.

Rao, C. R., L. L. Stowe, and P. McClain, Remote sensing of aerosols over oceans using AVHRR data, theory, practice and application, *Int. J. Remote Sens.*, *10*, 743–749, 1989.

Redemann, J., S. J. Masonis, B. Schmid, T. L. Anderson, P. B. Russell, J. M. Livingston, O. Dubovik, and A. D. Clarke, Clear-column closure studies of aerosols and water vapor aboard the NCAR C-130 in ACE-Asia, 2001, *J. Geophys. Res.*, *108*(D23), 8655, doi:10.1029/2003JD003442, in press, 2003.

Reid, S. J., T. F. Eck, S. A. Christopher, P. V. Hobbs, and B. Holben, Use of Angstrom exponent to estimate the variability of optical and physical properties of aging smoke particles in Brazil, *J. Geophys. Res.*, *104*, 27,473–27,489, 1999.

Remer, L. A., and Y. J. Kaufman, Dynamic aerosol model: Urban/industrial aerosol, *J. Geophys. Res.*, *103*, 13,859–13,871, 1998.

Remer, L. A., et al., Validation of MODIS aerosol retrieval over ocean, *Geophys. Res. Lett.*, *29*, 1–4, 2002.

Ricchiazzi, P., S. Yang, C. Gautier, and D. Sowle, SBDART: A research and teaching software tool for plane-parallel radiative transfer in the Earth's atmosphere, *Bull. Am. Meteorol. Soc.*, *79*, 2101–2114, 1998.

Russell, P. B., S. A. Kinne, and R. W. Bergstrom, Aerosol climate effects: Local radiative forcing and column closure experiments, *J. Geophys. Res.*, *102*, 9397–9408, 1997.

Russell, P. B., J. M. Livingston, P. Hignett, S. Kinne, J. Wong, A. Chien, R. Bergstrom, P. Durkee, and P. V. Hobbs, Aerosol-induced radiative flux changes off the U.S. mid-Atlantic coast: Comparison of values calculated from Sun photometer and in situ data with those measured by airborne pyranometer., *J. Geophys. Res.*, *104*, 2289–2307, 1999.

Schmetz, J., P. Pili, S. Tjemkes, D. Just, J. Kerkmann, S. Rota, and A. Ratier, An introduction to METEOSAT Second Generation (MSG), *Bull. Am. Meteorol. Soc.*, *81*, 977–1001, 2002.

Schmid, B., et al., Column closure studies of lower tropospheric aerosol and water vapor during ACE-Asia using airborne Sun photometer, airborne in situ and ship-based lidar measurements, *J. Geophys. Res.*, *108*(D23), 8656, doi:10.1029/2002JD003361, in press, 2003.

Schwartz, S. E., The Whitehouse effect—Shortwave radiative forcing of climate by anthropogenic aerosols, An overview, *J. Aerosol. Sci.*, *27*, 359–382, 1996.

Smirnov, A., B. N. Holben, T. F. Eck, O. Dubovik, and I. Slutsker, Cloud screening and quality control algorithms for the AERONET data base, *Remote Sens. Environ.*, *73*, 337–349, 2000.

Sokolik, I. N., A. Andronova, and T. C. Johnson, Complex refractive index of atmospheric dust aerosols, *Atmos. Environ.*, *27*, 2495–2502, 1993.

Tanré, D., Y. J. Kaufman, M. Herman, and S. Matto, Remote sensing of aerosol properties over oceans using the MODIS/EOS spectral radiance, *J. Geophys. Res.*, *102*, 16,971–16,988, 1997.

Tomasi, C., E. Caroli, and V. Vitale, Study of the relationship between Angstrom's wavelength exponent and Junge particle size distribution exponent, *J. Clim. Appl. Meteorol.*, *22*, 1707–1716, 1983.

Torres, O., P. K. Bhartia, J. R. Herman, A. Sinyuk, P. Ginoux, and B. Holben, A long-term record of aerosol optical depth from TOMS observations and comparison to AERONET measurements, *J. Atmos. Sci*, *59*, 398–413, 2002.

Wagener, R., S. Nemesure, and S. E. Schwartz, Aerosol optical thickness over oceans: High space- and time-resolution retrieval and error-budget from satellite radiometry, *J. Appl. Meteorol.*, *14*, 577–590, 1997.

Wang, J., S. A. Christopher, J. S. Reid, H. Maring, D. L. Savoie, B. Holben, J. Livingston, P. B. Russell, and S.-K. Yang, GOES 8 retrieval of dust aerosol optical thickness over the Atlantic Ocean during PRIDE, *J. Geophys. Res.*, *108*(D19), 8595, doi:10.1029/2002JD002494, 2003.

Welton, E. J., K. J. Voss, P. K. Quinn, P. Flatau, K. Markowicz, J. Campbell, J. D. Spinhirne, H. R. Gordon, and J. Johnson, Measurements of aerosol vertical profiles and optical properties during INDOEX 1999 using micropulse lidars, *J. Geophys. Res.*, *107*(D19), 8019, doi:10.1029/2000JD000038, 2002.

Zhang, J., S. A. Christopher, and B. Holben, Intercomparison of aerosol optical thickness derived from GOES-8 imager and ground-based Sun photometers, *J. Geophys. Res.*, *106*, 7387–7398, 2001.

Zhao, T. X.-P., L. L. Stowe, A. Smirnov, D. Crosby, J. Sapper, and C. McClain, Development of global validation package for satellite oceanic aerosol optical thickness retrieval based on AERONET observations and its application to NOAA/NESDIS operational aerosol retrievals, *J. Atmos. Sci.*, *59*, 294–312, 2002.

Zhou, J., G. Yu, C. Jin, F. Qi, D. Liu, H. Hu, Z. Gong, G. Shi, T. Nakajima, and T. Takamura, Lidar observations of Asian dust over Hefei, China, in spring 2000, *J. Geophys. Res.*, *107*(D15), 4252, doi:10.1029/2001JD000802, 2002.

F. Brechtel, Brechtel Manufacturing Inc., Hayward, CA 94544, USA. (fredb@bnl.gov)

S. A. Christopher and J. Wang, Department of Atmospheric Sciences, University of Alabama, 320 Sparkman Drive, Huntsville, AL 35805, USA. (sundar@nsstc.uah.edu; wangjun@nsstc.uah.edu)

B. N. Holben, Biospheric Sciences Branch, NASA Goddard Space Flight Center, Greenbelt, MD 20771, USA. (brent@spamer.gsfc.nasa.gov)

J. Kim, Meteorological Research Institute, Chungnam 357-961, South Korea. (jykim@metri.re.kr)

P. Quinn, PMEL, NOAA, 7600 Sand Point Way NE, Seattle, WA 98115, USA. (quinn@pmel.noaa.gov)

J. Redemann and B. Schmid, Bay Area Environmental Research Institute, Sonoma, CA 95476-6502, USA. (jredemann@mail.arc.nasa.gov; bschmid@mail.arc.nasa.gov)

P. B. Russell, NASA Ames Research Center, Moffett Field, CA 94035-1000, USA. (prussell@mail.arc.nasa.gov)

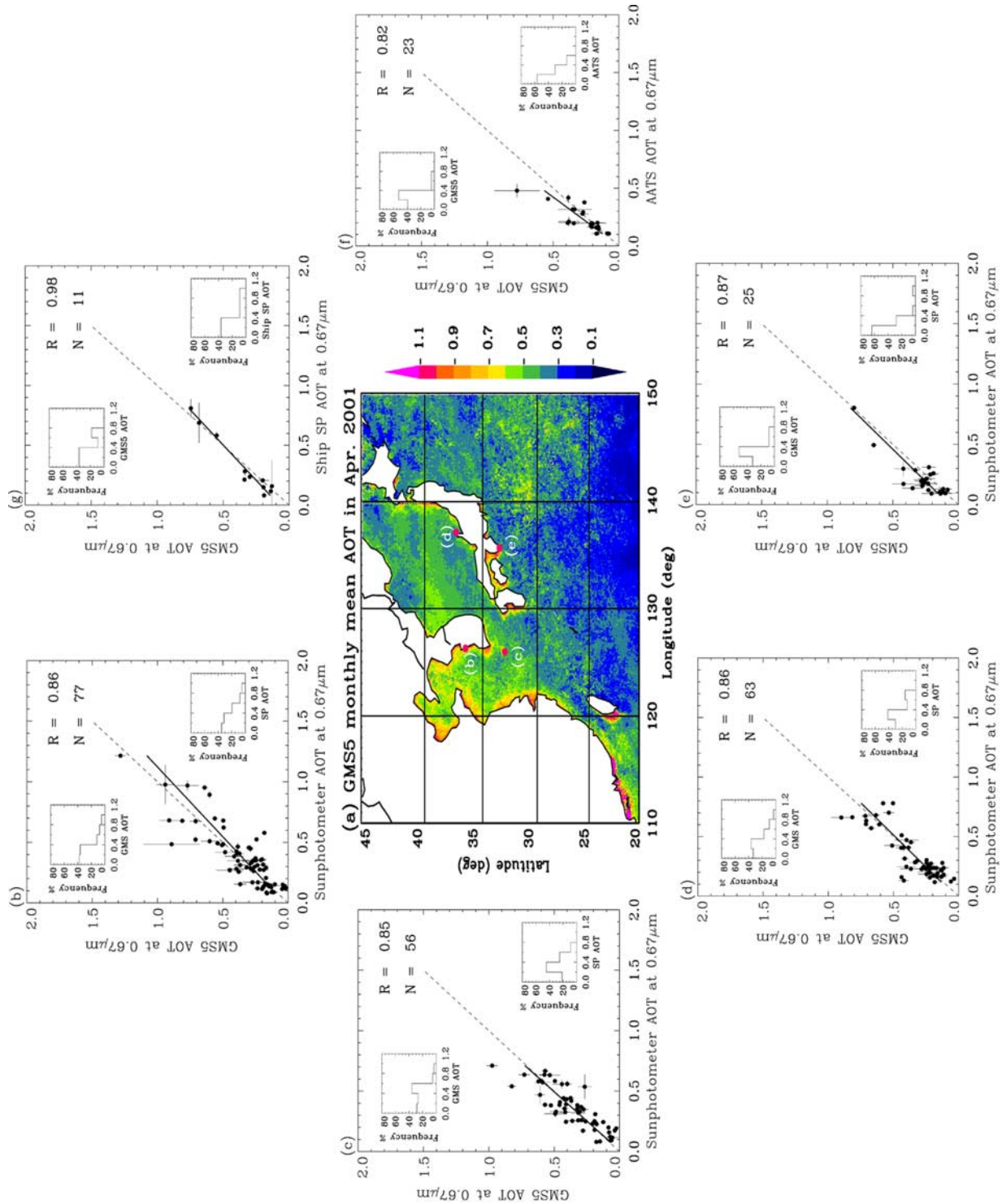

Figure 4. (a) Monthly mean GMS5 AOT and the comparison of GMS5 AOT with the AOT inferred from SP at (b) Anmyon and (c) Cheju, (d) Noto and (e) Shirahama as well as AOT inferred from (f) AATS6 and AATS14 and (g) ship SP. Letters b–e in Figure 4a shows the location of four AERONET sites Anmyon, Cheju, Noto, and Shirahama, respectively. Dotted line is the one-to-one correspondence and the solid line is the best fit to the points.